Figure S1.

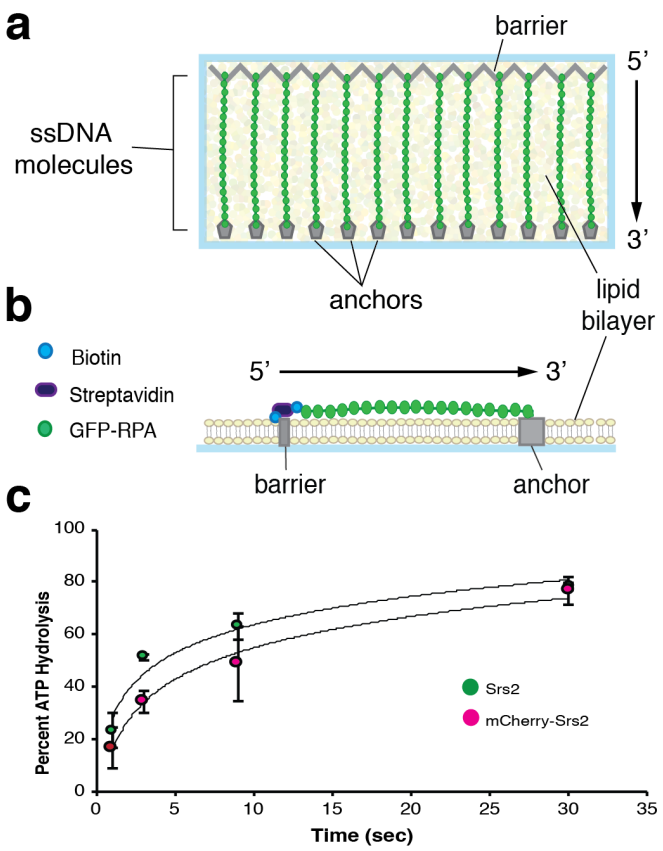

Figure S1. Single-stranded DNA curtain assay for Srs2 activity, Related to Figures 1 through 5. Schematic illustrations showing the **(a)** top and **(b)** side views of an ssDNA curtain. In these assays the ssDNA substrates are tethered to a supported lipid bilayer through a biotin-streptavidin linkage and then aligned at the leading edges of chromium (Cr) barriers to lipid diffusion. The ssDNA is then extended by addition of RPA, and then anchored though non-specific adsorption to Cr pedestals positioned downstream from the barriers. (**c**) Comparison of Srs2 and mCherry-Srs2 ATP hydrolysis activities in the presence of RPA-ssDNA. Data points represent the mean and standard deviation from three separate measurements.

Figure S2.

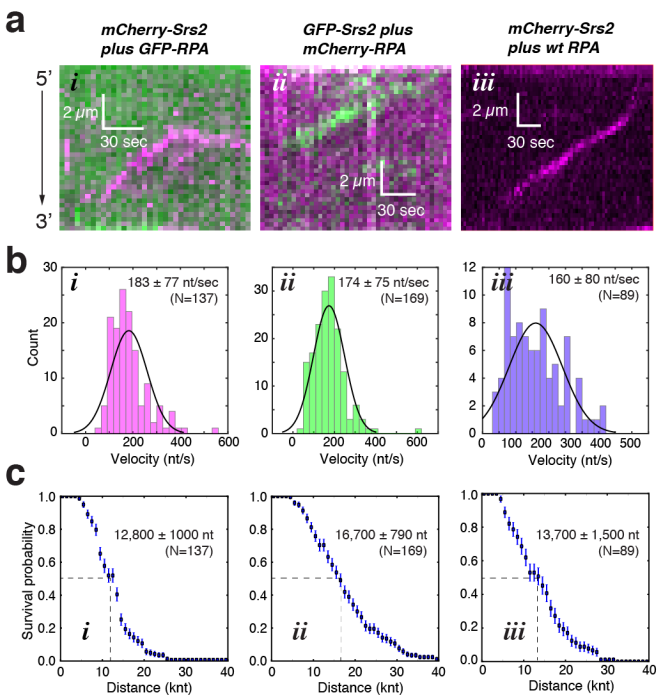

Figure S2. Translocation data for the different Srs2 and RPA constructs, Related to Figure 1. (a) Typical kymographs showing the behavior of (*i*) mCherry-Srs2 with GFP-RPA, (*ii*) GFP-Srs2 with mCherry-RPA, and (*iii*) mCherry-Srs2 with wild-type (unlabeled) RPA. **(b)** Velocity distributions and **(c)** survival probability data for each of the three different Srs2 and RPA combinations, as indicated; error bars represent s.d. calculated from bootstrapping analysis. Note that the data presented in Figures 1c & 1d of the main text represents the combination off all three of these independent data sets for Srs2 velocity and processivity.

Figure S3.

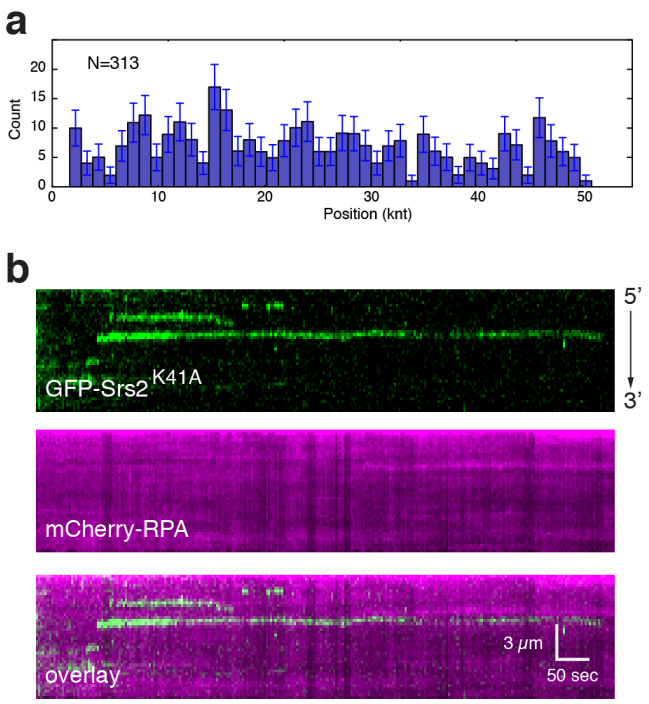

Figure S3. ATPase deficient mutant Srs2 K41A cannot translocate on RPA-ssDNA, Related to Figure 1. (a) Binding site distribution histogram of GFP-Srs2 K41A on mCherry-RPA-ssDNA. **(b)** Kymograph showing GFP-Srs2 K41A (green) bound to ssDNA coated with mCherry-RPA (magenta).

Figure S4.

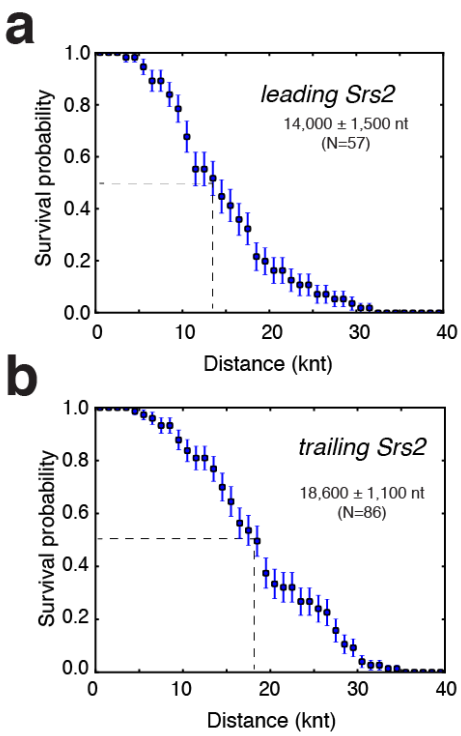

Figure S4. Srs2 processivity in the presence of bound Rad52, Related to Figure 5. Survival probability plots for the **(a)** leading and **(b)** trailing mCherry-Srs2 for experiments conducted with GFP-Rad52 bound to unlabeled RPA-ssDNA complexes; error bars represent s.d. calculated from bootstrapping analysis. There was no free Rad52 present in solution when Srs2 was injected.

Figure S5.

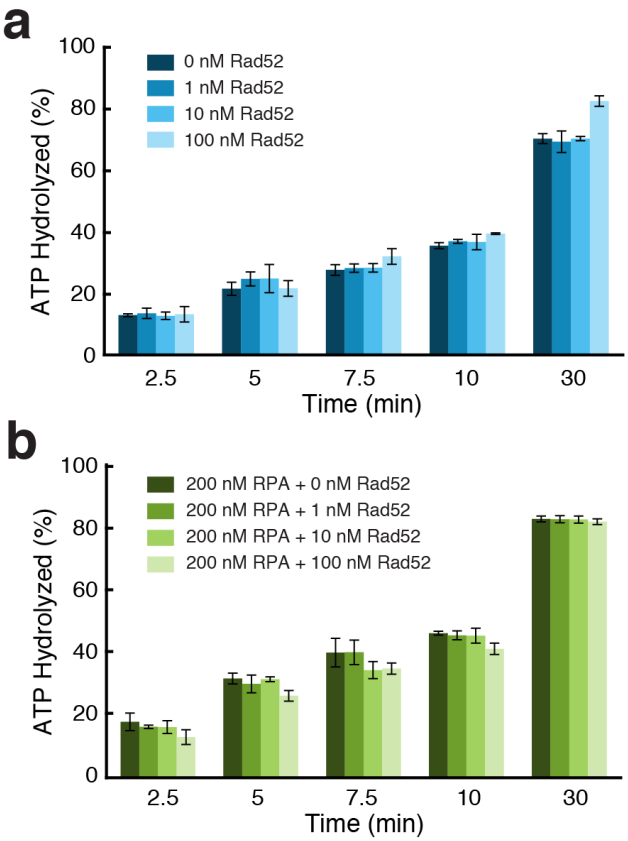

Figure S5. Rad52 does not inhibit Srs2 ATP hydrolysis activity, Related to Figure 5. (a) Srs2 ATP hydrolysis activity in the presence of ssDNA and increasing concentrations of Rad52. **(b)** Srs2 ATP hydrolysis activity in the presence of RPA-ssDNA and increasing concentrations of Rad52. Error bars represent s.d. based upon three independent experiments.

Figure S6.

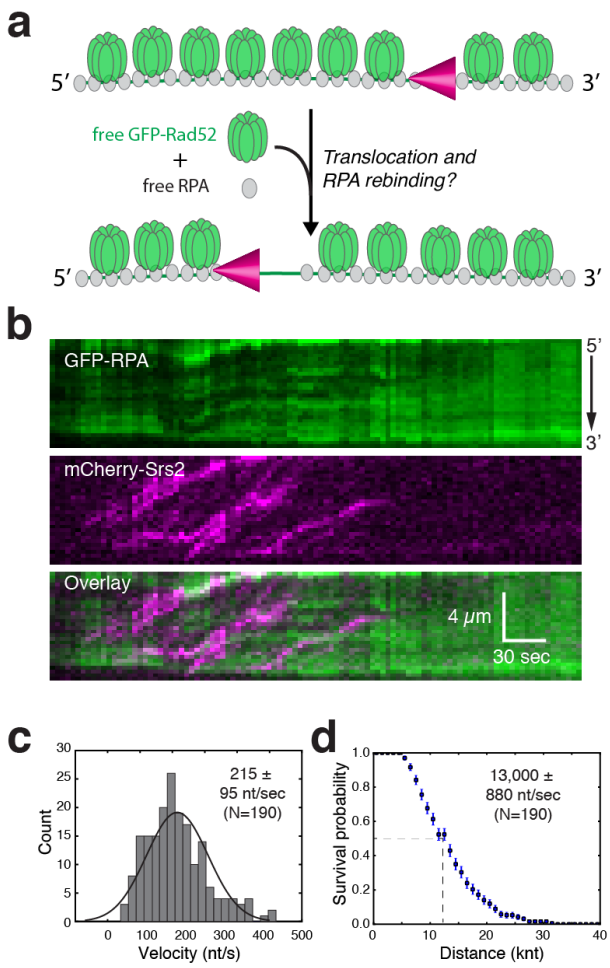

Figure S6. Srs2 promotes recycling of bound Rad52, Related to Figure 5. (a) Schematic for experiment to determine whether new GFP-Rad52 can rebind to the RPA-ssDNA complexes after passage of mCherry-Srs2. **(b)** Kymographs depicting examples of what takes place when mCherry-Srs2 acts upon unlabeled RPA-ssDNA in the presence of free and bound GFP-Rad52. During data collection, the reaction buffer contained 100 pM free RPA (unlabeled), and also contained 5 nM free GFP-Rad52. **(c)** Velocity distribution histograms and **(d)** survival probability graphs for Srs2 complexes taken from data collected in the presence of 5 nM GFP-Rad52.

Figure S7.

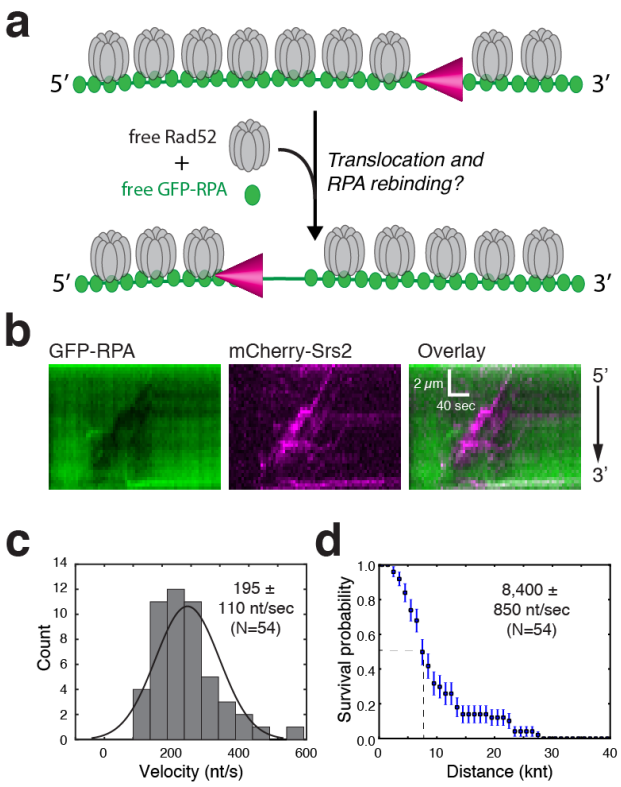

Figure S7. Srs2 promotes RPA recycling in the presence of free Rad52, Related to Figure 5. **(a)** Schematic for experiment to determine whether new GFP-RPA can rebind to the Rad52-RPA-ssDNA complexes after the passage of mCherry-Srs2. **(b)** Kymographs depicting examples of what takes place when mCherry-Srs2 acts upon Rad52-RPA-ssDNA in the presence of free and bound Rad52 (unlabeled). During data collection, the reaction buffer contained 100 pM free GFP-RPA, and also contained 5 nM free Rad52 (unlabeled). **(c)** Velocity distribution histograms and **(d)** survival probability graphs for mCherry-Srs2 complexes taken from data collected in the presence of 5 nM Rad52 present in solution.

SUPPLEMENTAL EXPERIMENTAL PROCEDURES

ATP hydrolysis assays

Comparison of unlabeled Srs2 and fluorescently-tagged Srs2 ATP hydrolysis activities was performed at 30˚C in HR buffer (30 mM Tris-Ac [pH 7.5], 50 mM KCl, 5 mM MgOAc, 1 mM DTT, 0.2 mg/ml BSA)(Figure S1c). Reactions contained 10 nM Srs2 (either unlabeled, or mCherry-tagged, as indicated), 10 nM RPA, 10 ng/ul circular single standed M13 DNA, 2 mM Cold ATP, and trace amounts of [γ-^{32}P]ATP. Aliquots were removed at specified time points and quenched with equal volume of 50 mM EDTA and 2% SDS. The quenched reactions were spotted on TLC (PEI-Cellulose, Millipore) plates and resolved in buffer containing 0.5 M LiCl and 1 M Formic acid. Dried TLC plates were exposed to phosphorimaging screen, and scanned with a Typhoon platform (GE Healthcare). Samples were quantified as the percentage of ATP hydrolyzed, and error bars represent the standard deviation of three independent experiments.

ATP hydrolysis assays testing for the effects of Rad52 (Figure S5) were performed in HR buffer (30 mM Tris-Ac [pH 7.5], 50 mM KCl, 5 mM MgOAc, 1 mM DTT, 0.1 mg/ml BSA, 2 mM ATP and 14 nM [γ-^{32}P]ATP (Perkin Elmer) and reactions were performed at 32˚C. All reactions contained M13 ssDNA (5 μM nucleotides; NEB), and the indicated concentrations of RPA, Rad52 or both. Reactions were initiated by the addition of 10 nM Srs2. Aliquots were removed at the indicated time intervals and quenched by the addition an equal volume of 500 mM EDTA. The quenched reactions were then spotted onto PEI (polyethyleneimine) TLC plates (Millipore) and resolved in buffer containing 0.5 M LiCl and 0.5 M formic acid. The TLC plates were then exposed to a phosphorous screen and imaged with a Typhoon platform (GE Healthcare). ATPase activity from minus Srs2 controls was subtracted as background. Values plotted were the mean of triplicate reactions with error bars representing standard deviation (s.d.).